Supporting Information for

Establishment of Structure-Conductivity Relationship for Tris(2, 2′-bipyridine)Ruthenium Ionic C_{60} Salts

*Jie Hong, Matthew P. Shores, and C. Michael Elliott**

Department of Chemistry, Colorado State University, Fort Collins, Colorado 80523-1872

Table of Contents

Figure S1. (a) The schematic design of four-probe conductivity measurement; **(b)** The homemade four-point probe apparatus.

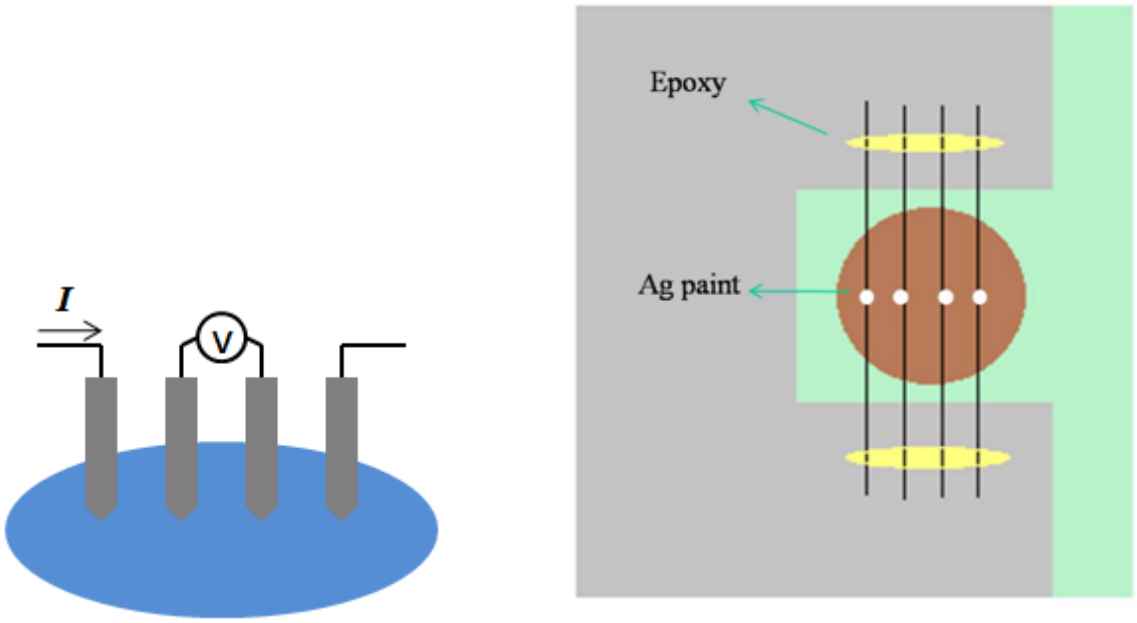

(**a**) (**b**)

Experimental

Four-probe Conductivity. The dc conductivity was measured on the central section of a circular pellet (radius = 3.5 mm) pressed at room temperature. Four tungsten wires (d = 75 μm) were lined parallel with equal spacing (Δ = 0.77mm ± 0.02 mm). A knot was tied in each wire and the knots were aligned in parallel. The knot on each tungsten wire was then coated with silver paint and serves as the contact. The apparatus was calibrated with Ba_2Te_3 prior to use. The following equation was used to calculate the bulk resistivity.[1]

$$\rho = C_s \times t \times R_S$$

$\boldsymbol{R_s}$ represents the sheet resistance which can be directly obtained from the I-V curve measured from the four-probe design. $\boldsymbol{t}$ is the thickness of thin sample sheet. The insulating KBr pellets were made

as substrates to support the fragile sample sheets. $\boldsymbol{C_s}$ is the correction factor which depends on the ratio of the diameter of thin sheet to the spacing of probes.[1] The value of $\boldsymbol{C_s}$ used is 4.17.[1] When measuring the sheet resistance $\boldsymbol{R_s}$, standard deviation σ_1 was obtained by multiple measurements with rotating the sample sheet to different positions. The thickness $\boldsymbol{t}$ was obtained by subtracting the thickness of KBr pellet (t_1) from the total thickness (t_2). The standard deviation σ_2 of $\boldsymbol{t}$ is a combination of error bars on t_1 and t_2. Finally, the standard deviation for bulk resistivity $\boldsymbol{\rho}$ was calculated to be around $\pm (|\sigma_1|+|\sigma_2|)$.

Figure S2. XPS survey spectra of (a) **1**, (b) **2** and (c) **3**.

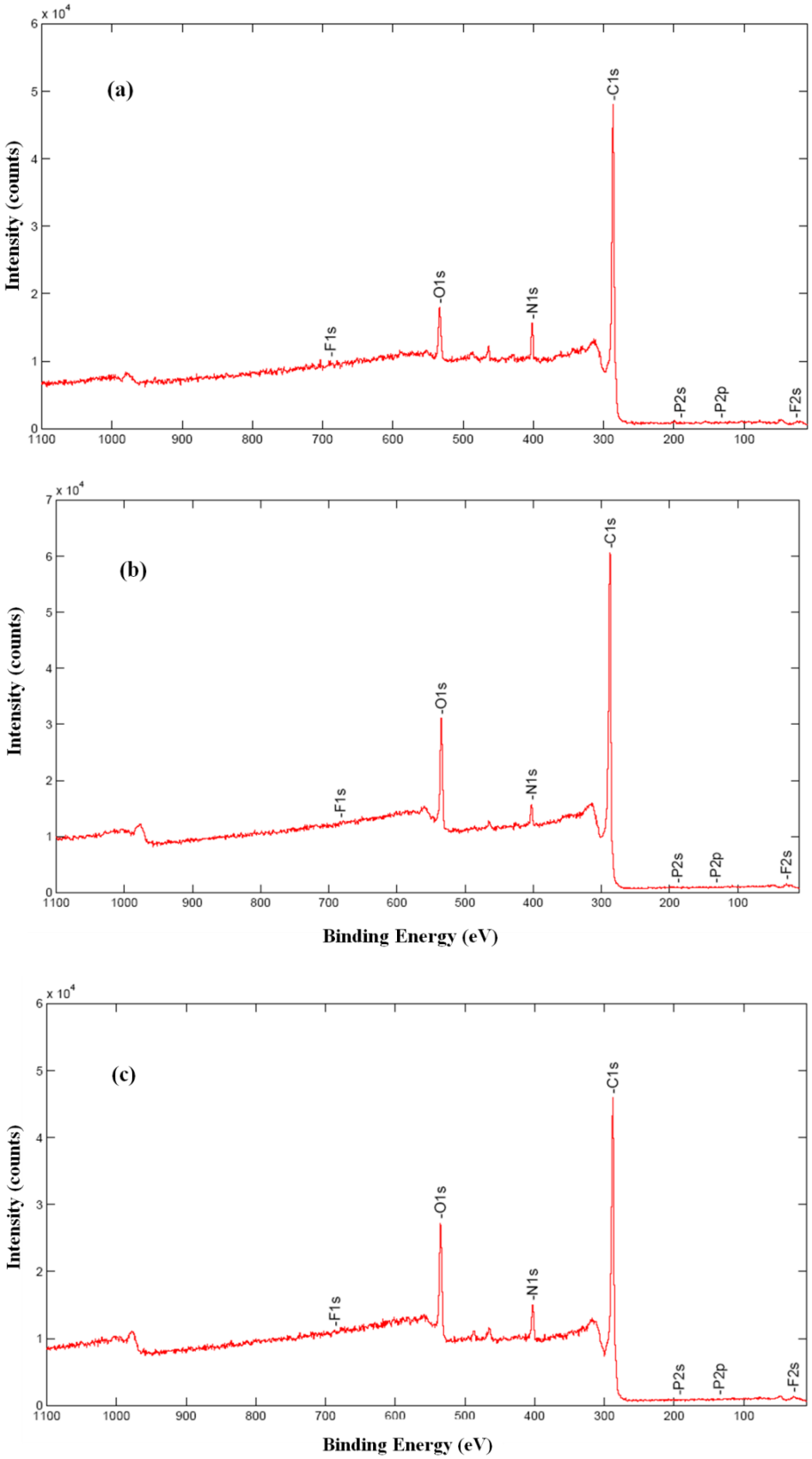

Figure S3. Asymmetric units of (**a**) crystal **1′** and (**b**) crystal **2′**.

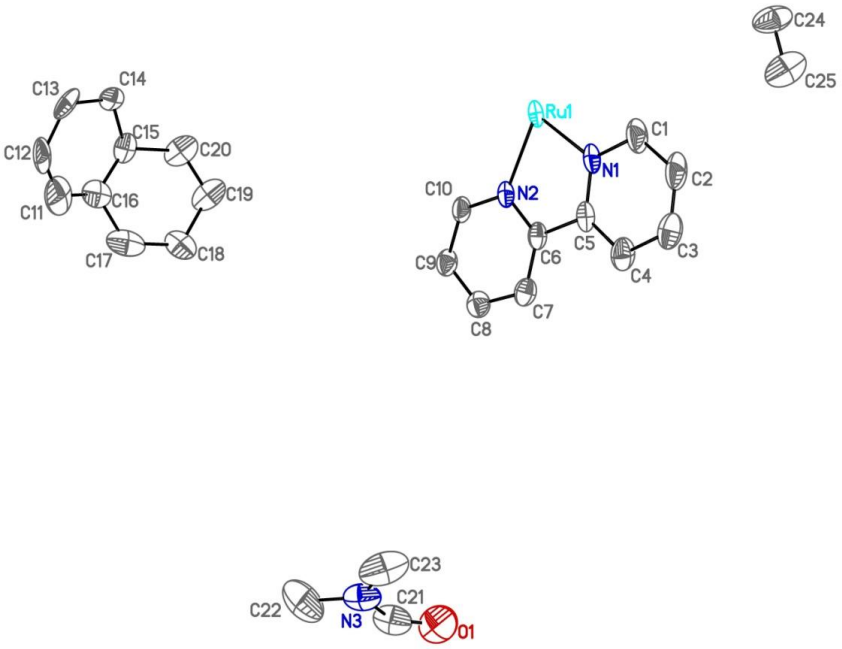

(**a**)

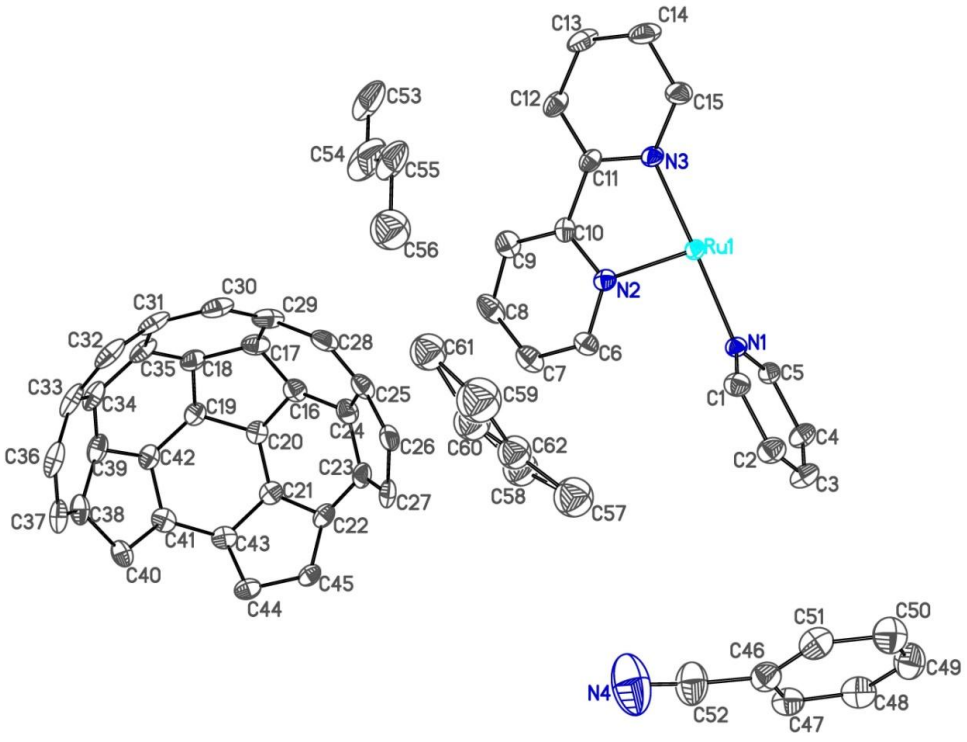

(**b**)

Figure S4. Temperature dependence of molar magnetic susceptibility (○) and the product of molar susceptibility and temperature (□) for compound **1** at 100 mT magnetic field**.**

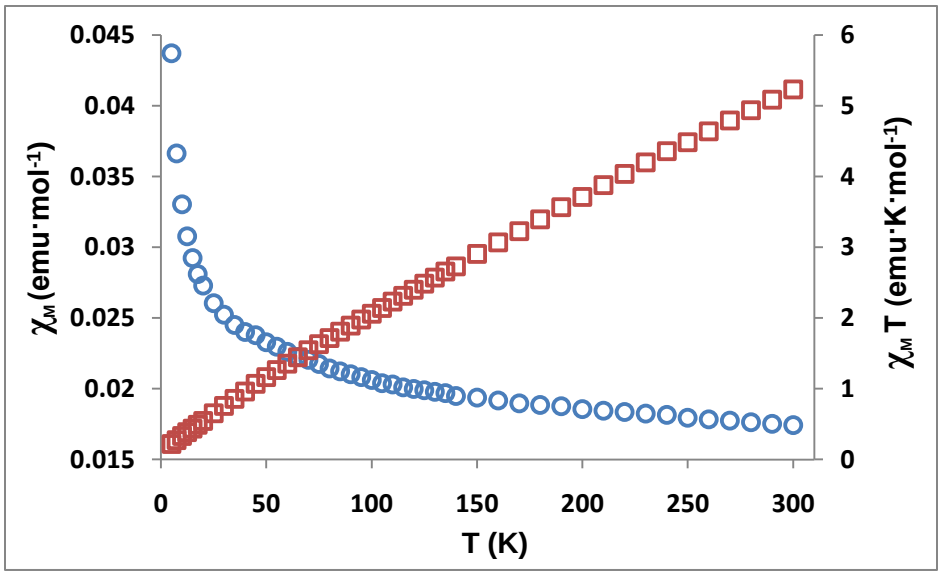

Figure S5. Temperature dependence of molar magnetic susceptibility (○) and the product of molar susceptibility and temperature (□) for compound **3** at 100 mT magnetic field**.**

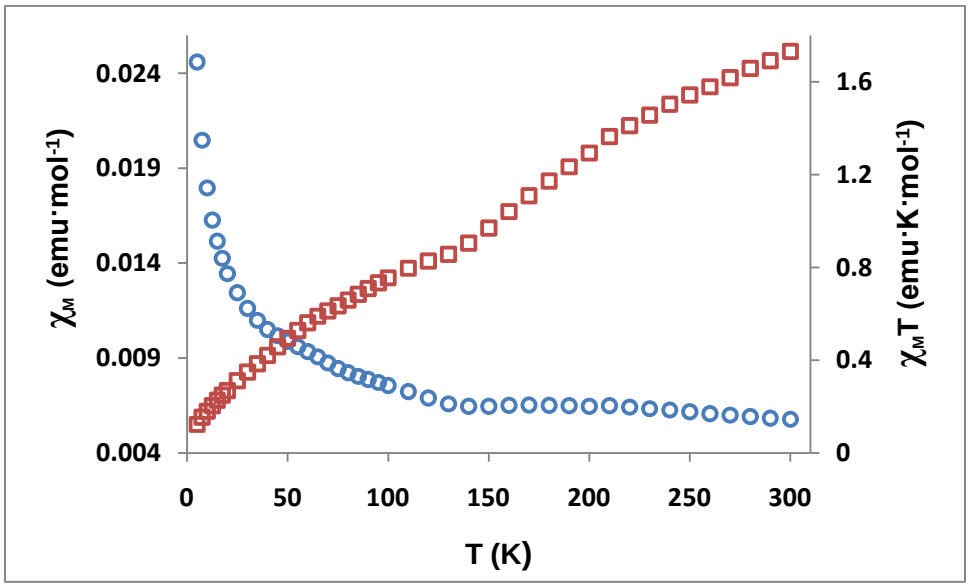

Experimental

Magnetic Susceptibility A Quantum Design MPMS-XL SQUID magnetometer was used to measure dc static susceptibilities of finely ground polycrystalline samples **1** and **3** between 300 and 5 K at 100 mT static magnetic fields. A sample holder contribution and diamagnetic susceptibility (χ_0) were subtracted from the experimental values. The value of χ_0 was obtained from literature,[2,3] which is in good agreement with the calculated value using Pascal's constants.[4] All of the data are reproducible on different batches of analytical pure samples.

Results and Discussion

For compound **1**, the product $\chi_M T$ behaves as a linear function of temperature (**Figure S4**). The data can be fit into the following equation.

$$\chi_M = \frac{C}{T} + \chi_{TIP}$$

There are two contributions to the overall magnetism. One of them is Curie paramagnetism and the other one is the so-called Van Vleck temperature-independent paramagnetism (TIP)[4] with χ_{TIP} = 15.9×10^{-3} emu·mol^{-1}. At 300 K, $\chi_M T$ was found to be 5.23 emu·K·mol^{-1} while the spin-only $\chi_M T$ value[4] should be 1.75 emu·K·mol^{-1} if we assume an S = ½ ground state for $[Ru(bpy)_3]^{1+}$ and S = 1 excited state for C_{60}^{2-}. The large difference is due to the large TIP, of which the origination is still not very clear. In alkali-metal doped C_{60}, χ_{TIP} was also observed but with a much smaller value (< 1 $\times 10^{-3}$ emu· mol^{-1}).[2] Since the HOMO and LUMO of $[Ru(bpy)_3]^{1+}$ and C_{60}^{2-} are of similar energy, the sizable experimental χ_{TIP} can be speculated to mainly arise from the Zeeman mixing of the ground state of $[Ru(bpy)_3]^{1+}$ and the abundant low-lying excited states in C_{60}^{2-}.[2,5-8] In addition, it is possible that the conduction electrons in compound **1** give rise to a positive temperature-

independent susceptibility as well.[2] At 5 K, the experimental value of $\chi_M T$ is 0.23 emu K mol^{-1} which is smaller than the spin-only value 0.75 {S = ½ for $[Ru(bpy)_3]^{1+}$ and S = 0 for C_{60}^{2-}}. This can be explained by the existence of a possible antiferromagnetic coupling (not ordering, as evidenced by the χ_M versus T plot) at low temperature. From single-crystal structural analysis, compound **1** shows possible close contact between adjacent $Ru(bpy)_3$•••$Ru(bpy)_3$ and adjacent $Ru(bpy)_3$•••C_{60}. Since the unpaired electron on $[Ru(bpy)_3]^{1+}$ does not reside in the metal center but actually in the π* orbital from the ligand,[7] the possible close contact makes antiferromagnetic coupling a possibility.

Solid sample **3** displays similar magnetic behavior to **1** but with a reduced $\chi_M T$ value and a small kink at 150-210 K (**Figure S5**). This kink may be due to a partial dimerization of C_{60}^{1-} units forming single-bonded diamagnetic $(C_{60}^{1-})_2$ dimers. This reversible phase transition of fullerene monoanion has been reported before in the similar temperature range.[9-12] Unfortunately, no structural data has been successfully obtained to confirm this speculation.

Overall, TIP seems to be a main contributor to the observed magnetism for both compound **1** and **3**. Both compounds do not show Curie-Weiss behavior but might have possible antiferromagnetic coupling at low temperatures. Furthermore, they do not represent magnetically isolated systems. To fully understand the magnetic properties, more studies need to be done in the future.

Figure S6. In single crystal **1′**, the positions of $Ru(bpy)_3^{m+}$ and C_{60}^{n-} in one unit cell. For simplicity, only Ru and N atoms were shown for $Ru(bpy)_3^{m+}$ sites.

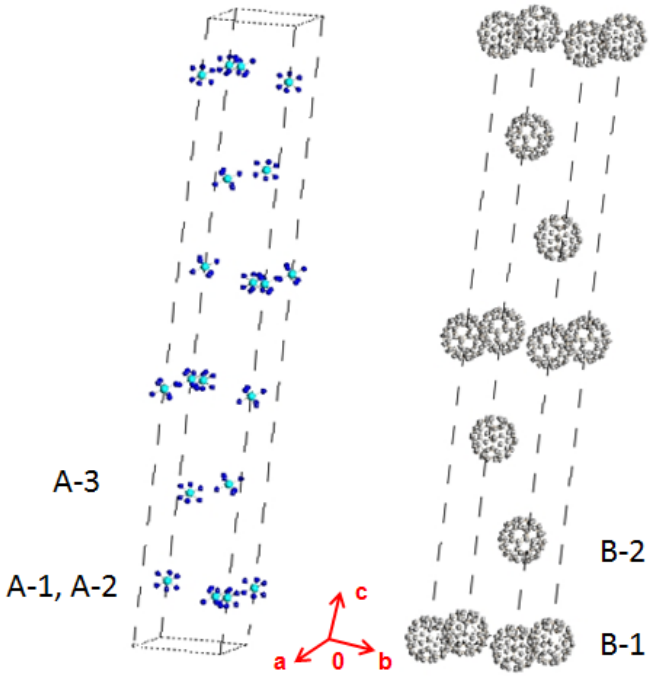

Figure S7. The surroundings of three types of $Ru(bpy)_3^{m+}$ sites (A-1, A-2, A-3) and two types of C_{60}^{n-} sites (B-1, B-2) in single crystal **1′**.

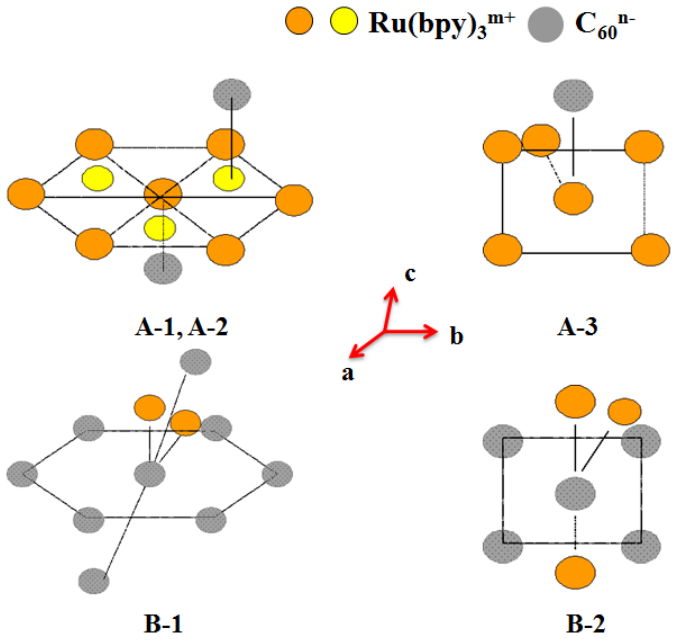

Figure S8. In single crystal **2′**, the positions of $Ru(bpy)_3^{m+}$ and C_{60}^{n-} in one unit cell. For simplicity, only Ru and N atoms were shown for $Ru(bpy)_3^{m+}$ sites.

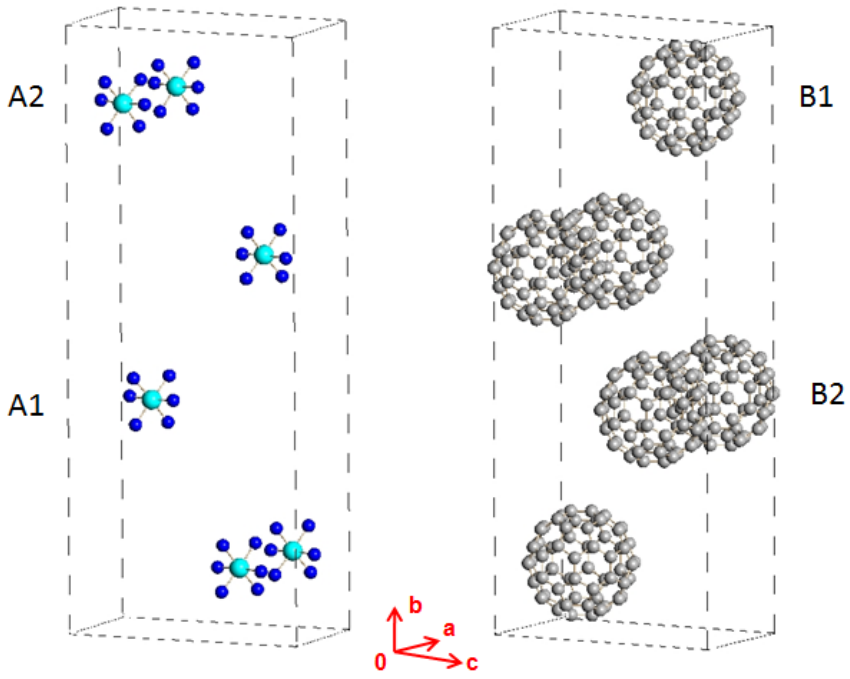

Figure S9. The surroundings of two types of $Ru(bpy)_3^{m+}$ sites (A1, A2) and two types of C_{60}^{n-} sites (B1, B2) in single crystal **2′**.

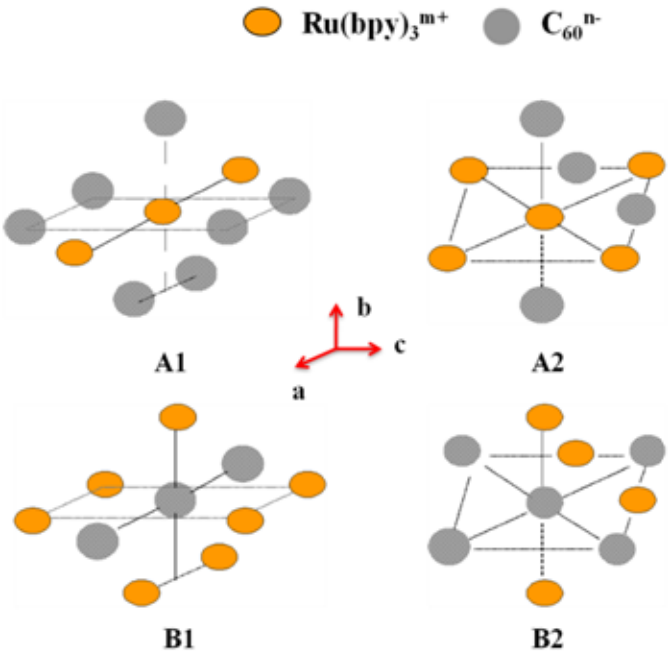

Figure S10. Visible-NIR spectra of compound **1** (**a**), **2** (**b**) and **3** (**c**) in solid state (red line) and in solution (black line).

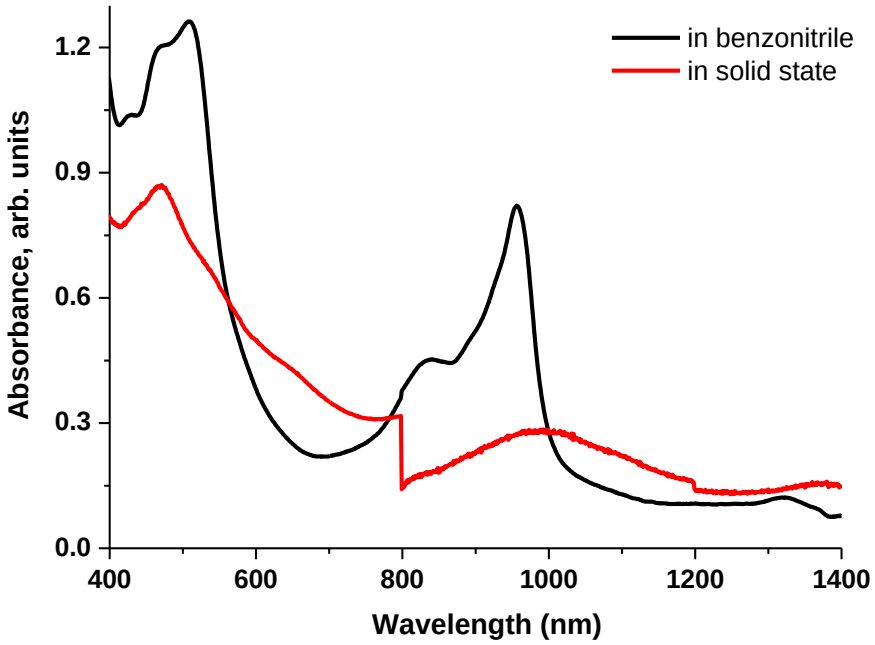

(**a**)

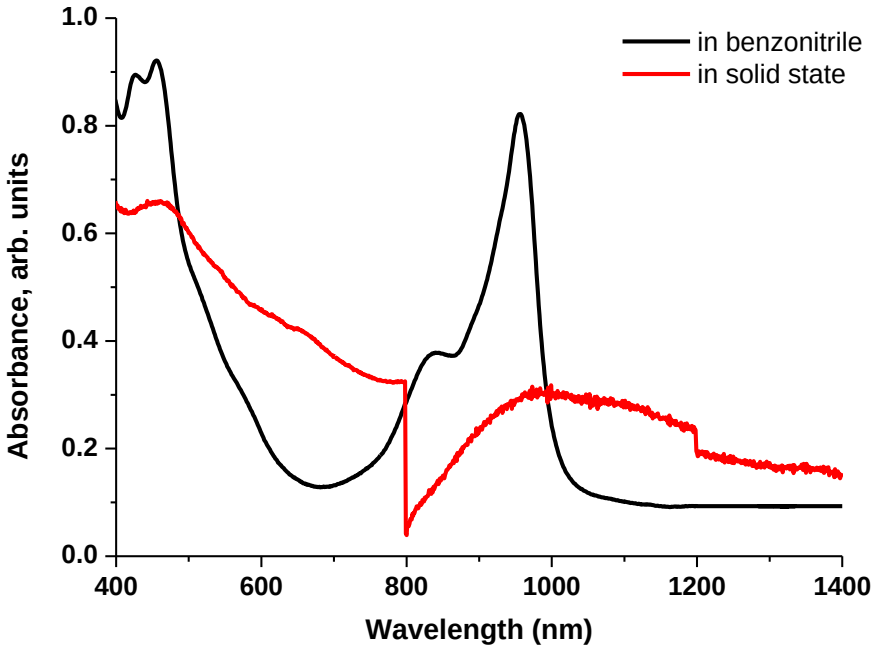

(**b**)

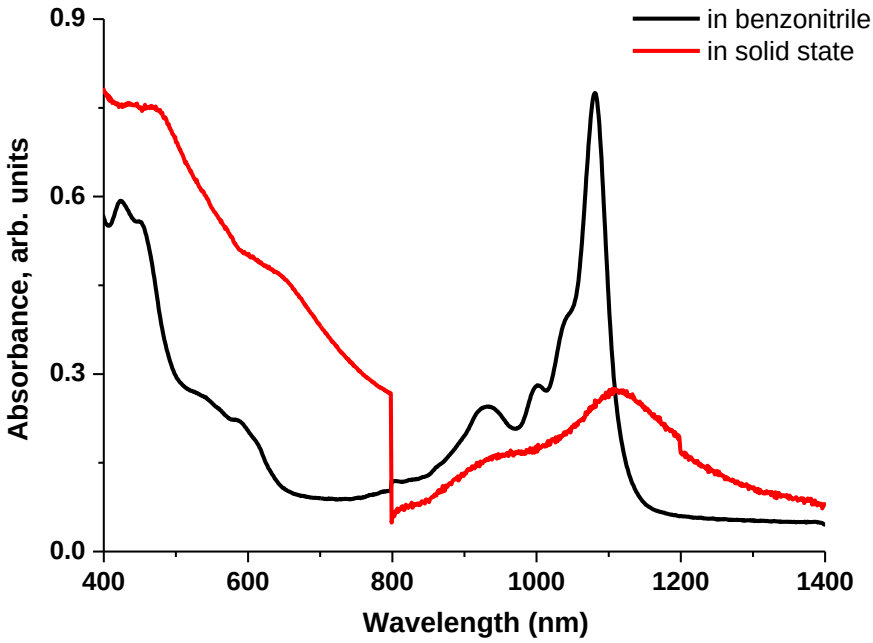

(**c**)

Experimental

Solid-state Visible-NIR Transmission Spectroscopy. In N_2-atmosphere glove box, small amount of solid sample was mixed well with finely ground FT-IR grade KBr powder. The mixtures were then pressed to be quasi-transparent pellets, in which the solid-state transmission spectra were measured from 400-1400 nm by Cary 500 UV-VIS-NIR spectrophotometer. The sharp spikes observed at 800 and 1200 nm are due to the grating change of spectrophotometer. As comparison, the corresponding solution spectra were included as black curves.

Table S1. Equations for calculating the relative concentrations of disproportionated redox species in compound **1** in solution with the assumption that $[Ru(bpy)_3^{m+}] = 2$ and $[C_{60}^{n-}] = 1$.

$$[RuL_3^{2+}]+[RuL_3^{1+}]+[RuL_3^{0}]=2$$

$$[C_{60}^{1-}]+[C_{60}^{2-}]+[C_{60}^{3-}]=1$$

$$2[RuL_3^{2+}]+[RuL_3^{1+}]=[C_{60}^{1-}]+2[C_{60}^{2-}]+3[C_{60}^{3-}]$$

$$E_{eq.} = E^0{}_{+1/+2} - \frac{RT}{F}\ln\frac{[RuL_3^{1+}]}{[RuL_3^{2+}]}$$

$$E_{eq.} = E^0{}_{0/+1} - \frac{RT}{F}\ln\frac{[RuL_3^{0}]}{[RuL_3^{1+}]}$$

$$E_{eq.} = E^0{}_{2-/1-} - \frac{RT}{F}\ln\frac{[C_{60}^{2-}]}{[C_{60}^{1-}]}$$

$$E_{eq.} = E^0{}_{3-/2-} - \frac{RT}{F}\ln\frac{[C_{60}^{3-}]}{[C_{60}^{2-}]}$$

The calculated equilibrium potential ($E_{eq.}$) in solution turned out to be right in the middle of the overlapped potential region of corresponding major $Ru(bpy)_3^{m+}$ and C_{60}^{n-}.

Table S2. Equations for calculating the relative concentrations of disproportionated redox species in compound **2** in solution with the assumption that $[Ru(bpy)_3^{m+}] = 1$ and $[C_{60}^{n-}] = 1$.

$$[RuL_3^{2+}] + [RuL_3^{1+}] + [RuL_3^{0}] = 1$$

$$[C_{60}^{1-}] + [C_{60}^{2-}] + [C_{60}^{3-}] = 1$$

$$2[RuL_3^{2+}] + [RuL_3^{1+}] = [C_{60}^{1-}] + 2[C_{60}^{2-}] + 3[C_{60}^{3-}]$$

$$E_{eq.} = E^0{}_{+1/+2} - \frac{RT}{F} \ln \frac{[RuL_3^{1+}]}{[RuL_3^{2+}]}$$

$$E_{eq.} = E^0{}_{0/+1} - \frac{RT}{F} \ln \frac{[RuL_3^{0}]}{[RuL_3^{1+}]}$$

$$E_{eq.} = E^0{}_{2-/1-} - \frac{RT}{F} \ln \frac{[C_{60}^{2-}]}{[C_{60}^{1-}]}$$

$$E_{eq.} = E^0{}_{3-/2-} - \frac{RT}{F} \ln \frac{[C_{60}^{3-}]}{[C_{60}^{2-}]}$$

Distribution of $Ru(bpy)_3^{3+}$ is negligible because the potential separation between $Ru(bpy)_3^{3+}$ and $Ru(bpy)_3^{2+}$ is large ($\Delta E > 2V$).

Table S3. Equations for calculating the relative concentrations of disproportionated redox species in compound **3** in solution with the assumption that $[Ru(bpy)_3^{m+}] = 1$ and $[C_{60}^{n-}] = 2$.

$$[RuL_3^{2+}] + [RuL_3^{1+}] + [RuL_3^{0}] = 1$$

$$[C_{60}] + [C_{60}^{1-}] + [C_{60}^{2-}] = 2$$

$$2[RuL_3^{2+}] + [RuL_3^{1+}] = [C_{60}^{1-}] + 2[C_{60}^{2-}]$$

$$E_{eq.} = E^0_{+1/+2} - \frac{RT}{F} \ln \frac{[RuL_3^{1+}]}{[RuL_3^{2+}]}$$

$$E_{eq.} = E^0_{0/+1} - \frac{RT}{F} \ln \frac{[RuL_3^{0}]}{[RuL_3^{1+}]}$$

$$E_{eq.} = E^0_{1-/0} - \frac{RT}{F} \ln \frac{[C_{60}^{1-}]}{[C_{60}]}$$

$$E_{eq.} = E^0_{2-/1-} - \frac{RT}{F} \ln \frac{[C_{60}^{2-}]}{[C_{60}^{1-}]}$$

Distribution of $Ru(bpy)_3^{3+}$ is negligible because the potential separation between $Ru(bpy)_3^{3+}$ and $Ru(bpy)_3^{2+}$ is large ($\Delta E > 2V$).

References

(1) Smits, F. M. *Bell Syst. Tech. J.* **1958**, *37*, 711-718.

(2) Dresselhaus, M. S.; Dresselhaus, G.; Eklund, P. C. *Science of Fullerenes and Carbon Nanotubes*; Academic Press: New York, 1996.

(3) Wagner, M. J.; Dye, J. L.; Perez-Cordero, E.; Buigas, R.; Echegoyen, L. *J. Am. Chem. Soc.* **1995**, *117*, 1318-1323.

(4) Kahn, O. *Molecular Magnetism*; Wiley-VCH, 1993.

(5) Negri, F.; Orlandi, G.; Zerbetto, F. *J. Am. Chem. Soc.* **1992**, *114*, 2909-2913.

(6) Hauser, A.; Amstutz, N.; Delahaye, S.; Sadki, A.; Schenker, S.; Sieber, R.; Zerara, M. *Struct. Bonding* **2004**, *106*, 81-96.

(7) Motten, A. G.; Hanck, K.; DeArmound, M. K. *Chem. Phys. Lett.* **1981**, *79*, 541-546.

(8) Peresie, H. J.; Stanko, J. A.; Mulay, L. N. *Chem. Phys. Lett.* **1975**, *31*, 392-394.

(9) Reed, C. A.; Bolskar, R. D. *Chem. Rev.* **2000**, *100*, 1075-1120.

(10) Konarev, D. V.; Khasanov, S. S.; Otsuka, A.; Saito, G. *J. Am. Chem. Soc.* **2002**, *124*, 8520-8521.

(11) Konarev, D. V.; Khasanov, S. S.; Vorontsov, I. I.; Saito, G.; Otsuka, A. *Synth. Met.* **2003**, *135-136*, 781-782.

(12) Konarev, D. V.; Khasanov, S. S.; Mukhamadieva, G. R.; Zorina, L. V.; Otsuka, A.; Yamochi, H.; Saito, G.; Lyubovskaya, R. N. *Inorg. Chem.* **2010**, *49*, 3881-3887.